A Journal of the Gesellschaft Deutscher Chemiker

Angewandte International Edition GDCh Chemie

www.angewandte.org

Accepted Article

Title: Dual Photosensitizer Coupled Three-Dimensional Metal-Covalent Organic Frameworks for Efficient Photocatalytic Reactions

Authors: Meng Lu, Shuai-Bing Zhang, Ming-Yi Yang, Yu-Fei Liu, Jia-Peng Liao, Pei Huang, Mi Zhang, Shun-Li Li, Zhong-Min Su, and Ya-Qian Lan

To be cited as: *Angew. Chem. Int. Ed.* **2023**, e202307632

Link to VoR: https://doi.org/10.1002/anie.202307632

WILEY VCH

10.1002/anie.202307632

RESEARCH ARTICLE

WILEY-VCH

Dual Photosensitizer Coupled Three-Dimensional Metal-Covalent Organic Frameworks for Efficient Photocatalytic Reactions

Meng Lu,[a]+ Shuai-Bing Zhang, [b]+ Ming-Yi Yang,[a]+ Yu-Fei Liu,[a] Jia-Peng Liao,[a] Pei Huang,[a] Mi Zhang,*[a] Shun-Li Li,[a] Zhong-Min Su[b] and Ya-Qian Lan*[a]

[a] Dr. M. Lu, M.-Y. Yang, Y.-F. Liu, J.-P. Liao, P. Huang, Dr. M. Zhang, Prof. S.-L. Li and Prof. Y.-Q. Lan
School of Chemistry
South China Normal University
Guangzhou, 510006, P. R. China.
E-mail: mizhang@m.scnu.edu.cn
E-mail: yqlan@m.scnu.edu.cn, Homepage: http://www.yqlangroup.com/

[b] S.-B. Zhang, Prof. Z.-M. Su.
School of Chemistry and Environment Engineering
Changchun University of Science and Technology
Changchun 130022, P. R. China.

[+] These authors contributed equally to this work.

Abstract: In this work, we innovatively assembled two types of traditional photosensitizers, that is pyridine ruthenium/ferrum ($Ru(bpy)_3^{2+}$/$Fe(bpy)_3^{2+}$) and porphyrin/metalloporphyrin complex (2HPor/ZnPor) by covalent linkage to get a series of dual photosensitizer-based three-dimensional metal-covalent organic frameworks (3D MCOFs), which behaved strong visible light-absorbing ability, efficient electron transfer and suitable band gap for highly efficient photocatalytic hydrogen (H_2) evolution. Rubpy-ZnPor COF achieved the highest H_2 yield (30338 μmol g^{-1} h^{-1}) with apparent quantum efficiency (AQE) of 9.68%@420 nm, which showed one of the best performances among all reported COF based photocatalysts. Furthermore, the in-situ produced H_2 was successfully tandem used in the alkyne hydrogenation with ~99.9% efficiency. Theoretical calculations reveal that both the two photosensitizer units in MCOFs can be photoexcited and thus contribute optimal photocatalytic activity. This work develops a general strategy and shows the great potential of using multiple photosensitive materials in the field of photocatalysis.

Introduction

Solar-to-chemical energy conversion to generate high-value-added chemicals from photocatalytic processes such as water splitting, carbon dioxide (CO_2) reduction, photocatalytic organic conversion and so on are known as green and promising strategies to resolve the energy crisis and environmental pollution over the world.[1] It is well known that the strong light absorption capacity, suitable optical band gap and band position alignments, efficient charge carrier mobility and restrain electron-hole recombination are all important factors for highly efficient photocatalysts that need to be considered comprehensively and synchronously, thus need rational and careful regulations.[2] In recent years, many inorganic semiconductors such as metal oxide, metal sulfide and metal nitride photocatalysts have been largely developed for photocatalysis.[3] The optical property of them can be adjusted by impurity doping, manufacturing defects, introducing heterojunction, and so on.[1a, 4] However, rationally and precisely regulating the above factors and understanding structure-activity relationships is still a great challenge due to the lack of a well-defined and precise catalyst structure model.[5] Especially, effective regulation of the visible light absorption ability, which is the priority of all factors, is highly desired for improving the photocatalytic performance that needs to be emphasis addressed.[6]

In the field of photocatalysis, metal-based molecular complex such as $Ru(bpy)_3^{2+}$, $Ir(ppy)_2(bpy)^+$, metalloporphyrin, and so on are traditionally strong photosensitizer (PS) and high frequency used for various photocatalysis due to the efficient electron transfer between PS and catalysts.[7] However, most of them only possess narrow visible light absorption ranges thus largely limiting their photocatalytic performance.[8] The introduction of second or more chromophore units into these molecular photosensitizer complexes has been proven to be an effective way to regulate their photosensitivity, which have realized extend the light absorption to visible even near-infrared range.[9] Up to now, some homogeneous multi-chromophore assembled molecule catalysts or PSs have been studied in this field, while still hard to realize the recycled and reused during the catalysis process.[10] Therefore, it is superior to develop an economical and practical heterogeneous photosensitive catalyst system for efficient photocatalysis.[11] Unfortunately, the multi-chromophore heterogeneous photosensitive system is rarely reported. In addition to this, it remains a great challenge to effectively couple multiple PS/chromophore together due to the lack of suitable conjunction method and such an integrated system demanding rigorous physical properties including efficient electro transfer and suitable band structure to fulfill the thermodynamic driving force for further photocatalytic reaction. [8a, 9b]

Crystalline organic photocatalysts integrated both the photophysical features of semiconductors and functional organic functional groups, also their structure is able to rationally design and precisely adjust through molecular engineering.[12,2C] Therefore, developing crystalline organic photocatalyst models with precise structures is a rational way to study photocatalytic processes and structure-functional relationships.[8a, 13] Covalent organic frameworks (COFs), a class of well-defined crystalline organic functional materials, with flexible structural designability and high stabilities are promising platforms for designing efficient photocatalysts.[14] More importantly, COFs offer the advantages of the molecular-level design of their optoelectronic properties owing to their precise structure frameworks.[14c, 15]

Herein, based on the reticular chemistry, [16] we developed a new strategy to implant two types of PS units, that is traditional metal-based molecular complex photosensitizer pyridine ruthenium/ferrum ($Ru(bpy)_3^{2+}$/ $Fe(bpy)_3^{2+}$) and porphyrin/metallo-

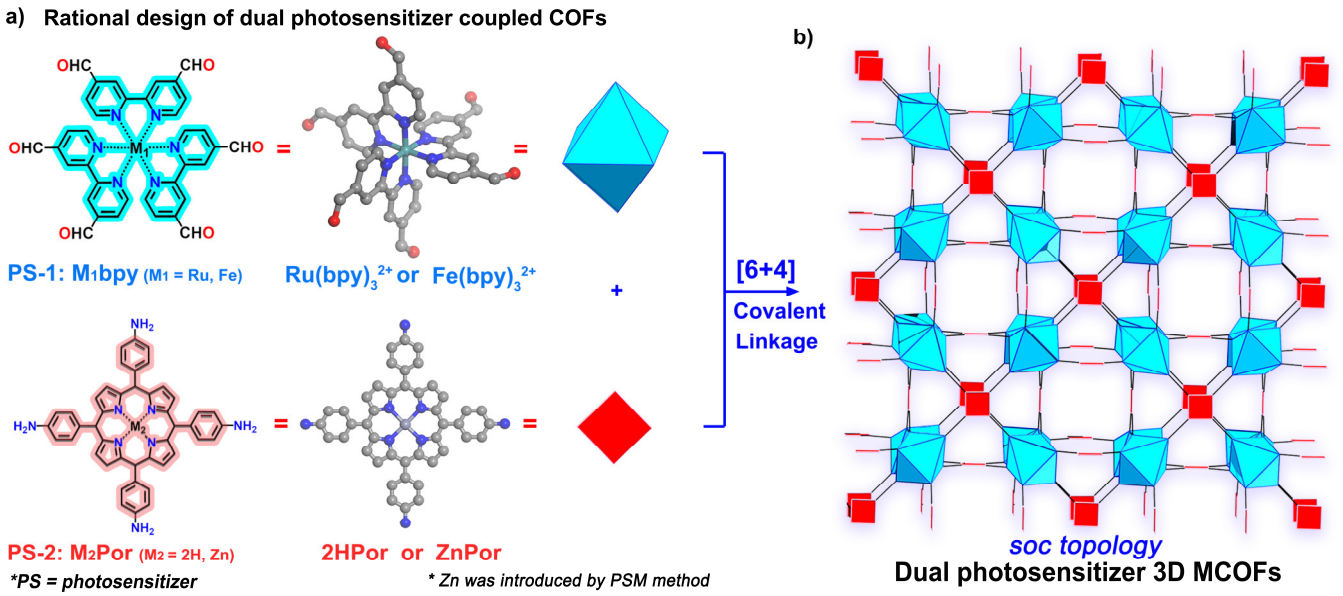

Scheme 1. a) Schematic of design and structure of dual photosensitizer 3D MCOFs by combining PS-1: M_1bpy (M_1 = Ru, Fe) and PS-2: M_2Por (M_2 = 2H, Zn) through [6+4] condensation by covalent linkage and **b**) the constructed soc topology frameworks. * PSM = post-synthesis method.

-porphyrin complex (2HPor/ ZnPor) together (Scheme 1a) via covalent linkage to form crystalline three-dimensional metal complex-based COFs (3D MCOFs) for photocatalysis. Specifically, we rationally designed a series of dual-photosensitizer based 3D MCOF photocatalysts including Rubpy-2HPor COF/Rubpy-ZnPor COF and Febpy-2HPor COF/ Febpy-ZnPor COF by condensing six- and tetratopic linkers to form imine-linked [6 + 4] 3D COFs with soc net topology (Scheme 1b).

In these photosensitive 3D MCOF photocatalysts, the co-sensitized and double photoexcited behavior boosts the photon-to-electron conversion efficiency, and the covalent bond is able to enhance electron transfer rates.[17] As a result, these synthesized 3D MCOFs combine the properties of a wide range of visible light-absorbing, efficient electron transfer, and have suitable band structures for visible light catalytic water splitting. Among them, the Rubpy-ZnPor COF showed the highest water splitting to hydrogen (H_2) rate of 30338 μmol g^{-1} h^{-1} with apparent quantum efficiency (AQE) of 9.68%@420 nm, which performed one of the best performances of all the reported COF-based photocatalysts. In addition, the in-situ produced H_2 was successfully tandemly used for organic hydrogenation reaction, which achieved >99.9% hydrogenation conversion efficiency for a series of alkyne substrates. Furthermore, the time-dependent density functional theory (TD-DFT) and spin density calculations demonstrated that the excited electronic state was localized on the Rubpy unit of Rubpy-ZnPor COF. In the process of photocatalysis, both the Rubpy and ZnPor can be excited by visible light irradiation, and subsequently electron transfer proceeded by two pathways then populated on Rubpy unit thus performing efficient H^+ reduction to H_2. This is the first report of multifold photosensitive based COF composites, and it is also of great significance in the field of photocatalysis catalysts.

Results and Discussion

As shown in Scheme 1a, a [6+4] covalent condensation reaction was applied to synthesize dual-photosensitizer based 3D MCOFs. Specifically, the Schiff-base condensation was applied between tris(4,4'-dicarboxaldehyde-2,2'-bipyridine) Ru/Fe (II) (abbreviated as M_1bpy, M_1 = Ru or Fe) and 5,10,15,20-tetrakis (4-aminophenyl)-porphinato] (abbreviated as 2HPor) and then introduced Zn (II) by PSM to form four 3D MCOFs, including Rubpy-2HPor COF/Rubpy-ZnPor COF and Febpy -2HPor COF/Febpy-ZnPor COF (Figure S1-3).

The structure of M_1bpy-M_2Por COF was first characterized by powder X-ray diffraction (PXRD) combined with theoretical structural simulation by using the Materials Studio package. In these reticular frameworks (Scheme 1 and Figure 1a, b), the octahedral M_1bpy units with six aldehyde groups acting as the 6-connected nodes and the square organic ligand M_2Por acting as the 4-connected building blocks, then formed an edge transitive (6, 4)-connected net. As shown in Figure 1a, b and Figure S60-61, M_1bpy occupy the eight vertices, while planar M_2Por units make up the six faces, forming a cubic cage. The vertices of each cubic cage are bedecked with 24 linking groups, thus assembling into 3D MCOFs. The soc topology structure model based on M_1bpy-M_2Por COF was built and the experimental PXRD diffraction patterns matched with the calculated results.[18] Besides, the stp topology structural models were also built (Figure. S62), however, the PXRD which was calculated from stp and 2-fold stp topology were found to be fully inconsistent with the experimental ones (Figure. S63), thus ruling out the possibilities of stp topology.[19] Structural analysis via PXRD reveals that both the COFs are crystalline and showed peak positions at 2θ = 4.41, 5.12, 5.78, 7.42, 10.64 and 11.32, which can be assigned to the 200, 211, 220, 222, 422 and 510 reflections in the simulated raw structural model, respectively. However, the main peaks of them perform differently, where the Rubpy-2HPor COF showed main peak at 211 faces, while Febpy-2HPor COF shows main reflections at 200 faces, which may be caused by preferred orientations of crystals. Therefore, the preferred orientation simulation was also included in the structure refinement process. We then carried out both Pawley and Rietveld refinements[20] based on the PXRD patterns for full profile fitting against the proposed structure models to optimize the lattice parameters and crystal structure. As a result, the

Pawley refinements of PXRD patterns fitted well with the experimental results with residuals of *Rp*= 4.13%/ *Rwp*= 7.31% for Rubpy-2HPor COF and *Rp*= 6.21%/ *Rwp*= 7.89% for Febpy-2HPor COF (Figures 1c and 1d). Furthermore, the Rietveld refinement for Rubpy-2HPor COF and Febpy-2HPor COF fitted with the experimental results with convergence to Rp=6.29%/ Rwp=9.58% and Rp=6.81%/ Rwp=9.79%, respectively (Figures S58-59). These structure refinements finally provided a unit cell parameter of a=b=c= 42.7452 Å and α=β=γ=90° for Rubpy-2HPor COF with *I432* cubic space group and a=b=c= 41.7302 Å and α=β=γ=90° for Febpy-2HPor COF (Figures S64-65).[21] The comparison of PXRD patterns of COFs with those of monomers was also conducted (Figures S4-5), which proved the purity of these 3D MCOFs. Besides, the PXRD patterns of Rubpy-ZnPor COF and Febpy-ZnPor COF also matched well with the calculated results (Figure S6-7).

The formation of the Schiff-base linkages in these 3D COFs was first confirmed by Fourier transform infra spectroscopy (FT-IR). The appearance of a new peak at 1623 cm^{-1} in FT-IR can be the assignment to the telescopic vibration of the imine bond (-C=N) (Figure 1e and Figure S8-10).[22] The solid-state ^{13}C cross polarization magic angle spinning(^{13}C CP/MAS) NMR spectroscopy showed a clear peak at 159 ppm which is

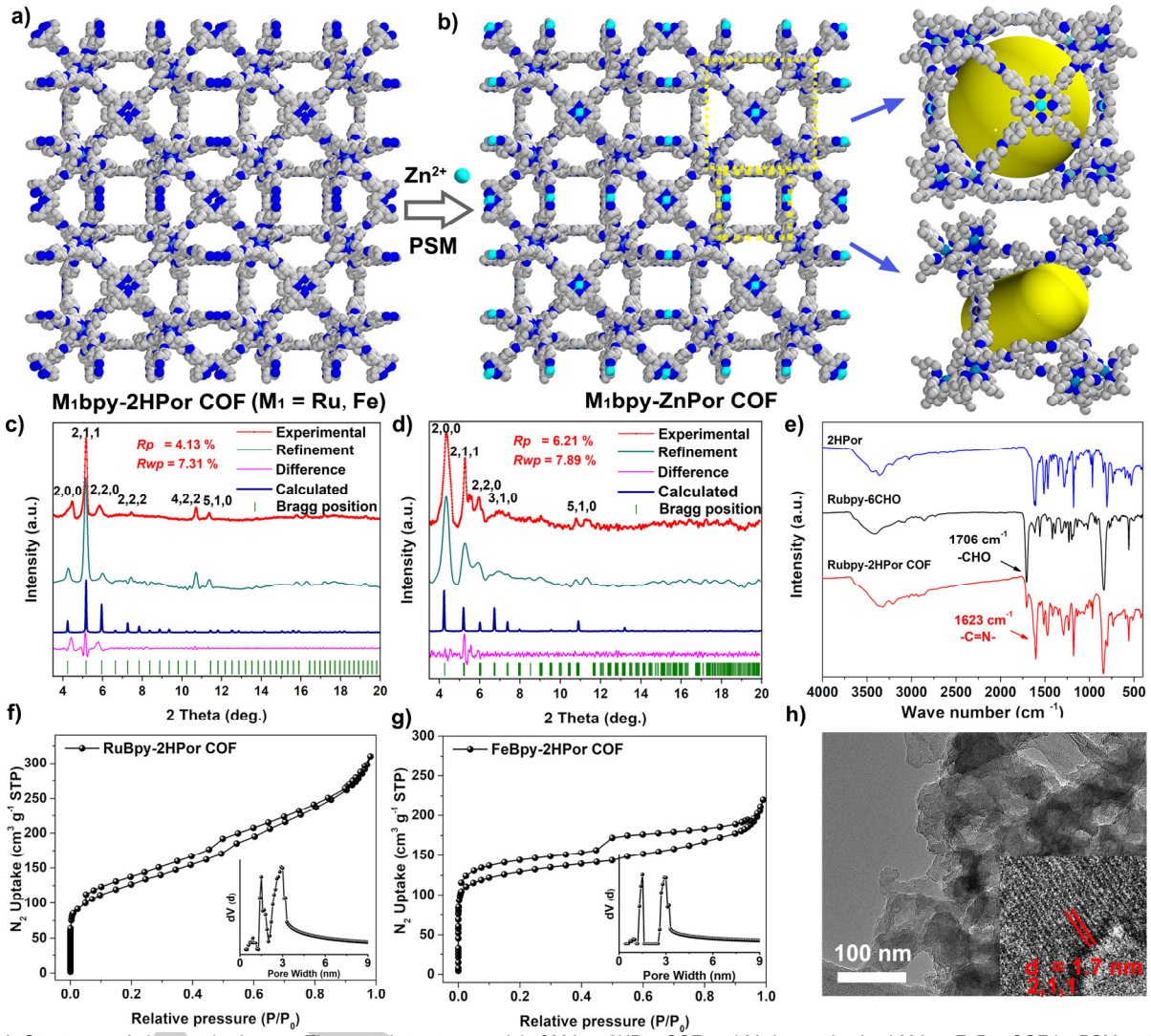

Figure 1. Structure and characterizations. **a**) The crystal structure model of M_1bpy-2HPor COF and **b**) the synthesized M_1bpy-ZnPor COF by PSM and the unit cubic cage and tunnel of COFs (The PF_6^- anions are eliminate for clarity). **c**) The experimental and simulated PXRD patterns of Rubpy-2HPor COF and **d**) Febpy-2HPor COF. **e**) FT-IR spectrum. The N_2 adsorption isotherm and pore size distribution of **f**) Rubpy-2HPor COF and **g**) Febpy-2HPor COF. **h**) The TEM and HRTEM of Rubpy-2HPor COF.

attributed to the carbon of the imine bond (Figure S11-14).[23] All these results confirmed the successful covalent condensations required for M_1bpy-M_2Por COF. The nitrogen adsorption-desorption isotherms measurement at 77 K was conducted and we can observe a sharp gas uptake at low relative pressures (Figure 1f, g and S15-16). A pore width distribution centered at ~1.5 and ~2.7-2.9 nm was calculated from the nonlocal density functional theory (NL-DFT) method, which is in accordance with the predicted structure. The Brunauer-Emmett-Teller (BET) surface area of Ru/Febpy-2HPor COF and Ru/Febpy-ZnPor COF is 537.50, 436.3, 541.42, 460.76 m^2 g^{-1}, respectively. The relatively low surface area may contribute to the PF_6^- ions dispersing in the pores of 3D MCOFs.[24] We also test the CO_2 adsorption of these COFs and the isotherm curve is shown in Figure S17-18. The CO_2 adsorption capacity of them is 31.1, 20.2, 22.7, and 13.7 cm^3 g^{-1}, respectively. These results confirm the permanent porosity structure of COFs. Scanning electron microscopy (SEM) and transmission electron microscopy (TEM) were performed to characterize the morphology of M_1bpy-M_2Por COF, which showed that these 3D MCOFs composed of

microcrystalline particles with 100–200 nm in diameter (Figure 1h and Figure S19-23). The structural characteristics of these MCOFs were then visualized by high-resolution transmission electron microscopy (HRTEM). As shown in the inset image of Figure 1h, Rubpy-2HPor COF displayed clear lattice fringes of (211) crystal face with *d*-spacing of 1.7 nm, which also confirmed the rationality of the simulated crystal structure. The chemical stability was studied, and the PXRD and FT-IR results showed that the Rubpy-2HPor COF were stable in common organic solvents (tetrahydrofuran (THF), methanol (MeOH), acetonitrile (ACN)) for 3 days (Figure S24-25). We then performed X-ray photoelectron spectroscopy (XPS), inductively coupled plasma (ICP), and thermo gravimetric analysis (TGA) to study the structural properties of these 3D MCOFs. High-resolution XPS measurements were conducted and the analysis results showed the divalent state of the Ru/Fe of bipyridine complex and Zn in the porphyrin pocket of MCOFs (Figure S26–S31). The TGA results showed that these COFs could be stable up to ca. 200 °C under O_2 and start to sharply weight loss at ca. 300 °C, which is caused by the decomposition of COFs (Figure S32–S39). The ICP analysis revealed that the Ru and Zn mass content in Rubpy-ZnPor COF is 5.13 and 5.09 wt.%, which is close to the theoretical value under complete coordination (5.82 and 5.64 wt.% for Ru and Zn in Rubpy-ZnPor COF, calculated from moiety formula $C_{204}H_{120}N_{36}Ru_2Zn_3$). In addition, the details of the structure and characterization of Rubpy-ZnPor COF and Febpy-ZnPor COF are further discussed in the Supporting Information.

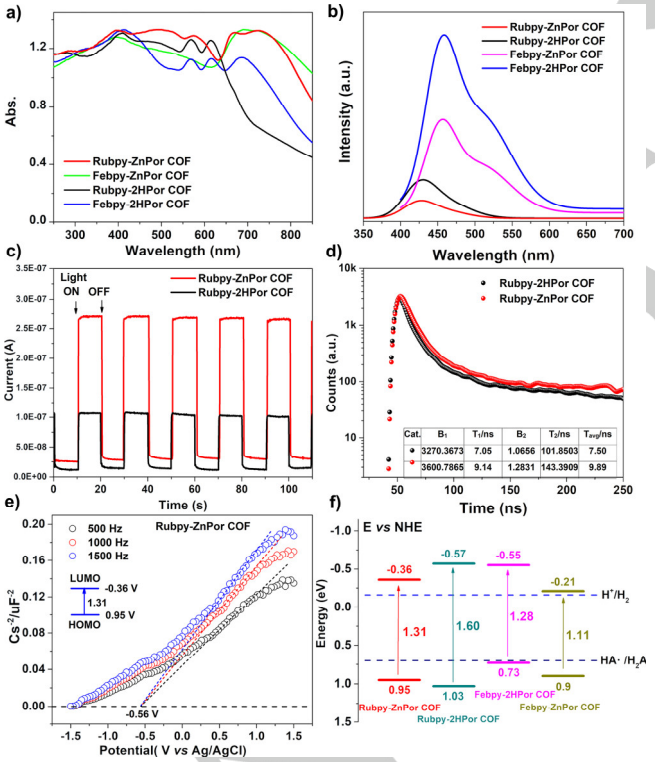

Figure 2. Optical characterization. **a)** Solid-state UV/Vis absorption spectrum and **b)** PL spectrums. **c)** Transient photocurrent response and **d)** The fluorescence lifetime of Rubpy-ZnPor COF and Rubpy-2HPor COF. **e)** Mott–Schottky plot of Rubpy-ZnPor COF. **f)** Band-structure diagram for COFs.

The optical physics characterizations including ultraviolet-visible (UV/Vis) light adsorption ability, photoluminescence spectroscopy (PL) and lifetime decay, transient photocurrent response, and band structure were first studied to investigate the features of these MCOFs for potential photocatalytic applications. The solid-state UV/Vis absorption results reveal that all these MCOFs especially Rubpy-ZnPor COF and Febpy-ZnPor COF possess strong visible light absorption capacity (Figure 2a and Figure S40-45) and the absorption range covered almost all visible regions. The PL and time-resolved fluorescence decays were studied to investigate the charge separation behaviors (Figure 2b, d, and S47). Interestingly, the PL intensity of Rubpy-ZnPor COF was significantly quenched compared to the other three COFs. At the same time, Rubpy-ZnPor COF has the longest average fluorescence lifetime (t_{avg} = 9.89 ns), suggesting efficient charge separation efficiency.

Furthermore, the intensity of the transient photocurrent response showed that Rubpy-ZnPor COF owns the highest intensity than other COFs (Figure 2c and S46), which suggested superior photoinduced electron separation and transport efficiency. The Mott-Schottky (MS) measurements were then conducted to determine the electronic band positions of the as-prepared materials (Figures 2e and S48–S50). The test results showed that the conduction-band position is -0.36 V (vs. Normal Hydrogen Electrode, NHE) for Rubpy-ZnPor COF (Figures 2f). Combined with the band gap calculated from UV/Vis absorption, the valence-band position can be determined as 0.95 V.

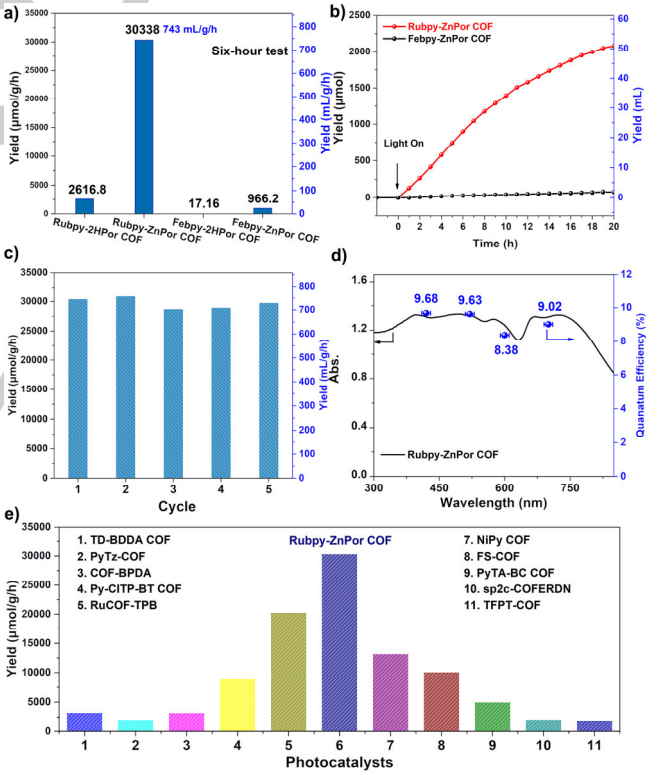

Figure 3. Photocatalytic H_2 evolution performance. **a)** Comparation of photocatalytic H_2 evolution activity. **b)** Time-dependent H_2 yield performance. **c)** Durability measurements. **d)** Wavelength-dependent AQE of photocatalytic H_2 evolution. **e)** Performance comparison of Rub-py-ZnPor COF with reported representative COF photocatalysts.

Theoretically, a more negative lowest unoccupied molecular orbital (LUMO) level than the H^+/H standard reduction potential and a more positive highest occupied molecular orbital (HOMO) level than the $HA^{\cdot}/H_2A$ (L-ascorbic acid) standard oxidation potential for a photocatalyst are needed to catalyze the H^+ reduction to H_2 with H_2A as the electron donor. Interestingly, the

band-structure diagram demonstrated that all these 3D MCOFs meet the requirements of the above two half-reactions. Furthermore, the water contact test showed that these 3D MCOFs are all hydrophilicity (Figure S51-52), which is beneficial to the photocatalytic water splitting reaction. Based on the above illustration of the structure and features, it can be proposed that the covalently linked two photosensitizers coupled COFs will have great potential for photocatalytic reactions.

We then studied the photocatalytic H_2 evolution performance of these 3D MCOFs by using platinum as a co-catalyst. After screening the photocatalytic conditions, the highest H_2 yield was observed in the Rubpy-ZnPor COF with 30338 μmol g^{-1} h^{-1}, which is 31 times higher than Febpy-ZnPor COF (966.2 μmol g^{-1} h^{-1}) and ~12 times higher than Rubpy-2HPor COF (2616.8 μmol g^{-1} h^{-1}) (Figure 3a). It is noted that Febpy-2HPor COF only showed little activity for H_2 evolution, which may be due to it possessing a very closed HOMO level to $HA^{\cdot}/H_2A$ redox potential, thus suggesting unfavorable thermodynamically for $HA^{\cdot}/H_2A$ oxidation. A time-dependent hydrogen evolution experiment was then conducted. The H_2 production exhibited a linearly increasing tendency at the first ~10 h and then tardily mitigate due to the continually consume of sacrificial agents (ascorbic acid) (Figure 3b). We also tested the water-splitting performance of the precursors (Rubpy/Febpy and Por/ZnPor monomers) of these MCOFs, and the results showed that all these building units only performed low H_2 evolution activity (Figure S53), while after formed COF composites, the water-splitting activity greatly improved. More importantly, the covalently linked Rubpy-ZnPor COF showed much higher activity than the physical mixing of components (named Rubpy/ZnPor, 1390 μmol g^{-1} h^{-1}), proving the validity of the covalent connection. Additionally, the activity of Rubpy-ZnPor COF catalyst can maintain at least five cycles without obvious decay (Figure 3c).

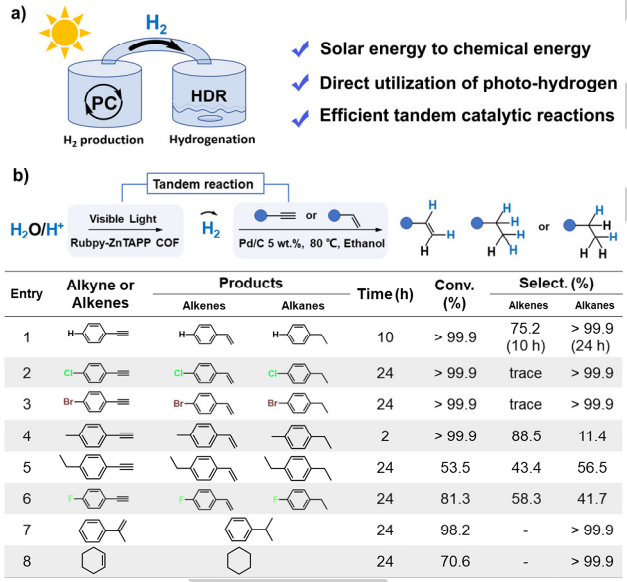

Entry	Alkyne or Alkenes	Products		Time (h)	Conv. (%)	Select. (%)	
		Alkenes	Alkanes			Alkenes	Alkanes
1				10	> 99.9	75.2 (10 h)	> 99.9 (24 h)
2				24	> 99.9	trace	> 99.9
3				24	> 99.9	trace	> 99.9
4				2	> 99.9	88.5	11.4
5				24	53.5	43.4	56.5
6				24	81.3	58.3	41.7
7				24	98.2	-	> 99.9
8				24	70.6	-	> 99.9

Figure 4. a) Schematic of photocatalytic H_2 production in tandem with organic hydrogenation. **b)** The performance of photocatalytic H_2 production in tandem with organic hydrogenation. Reaction conditions: Chamber A (H_2 evolution): COF (5 mg), H_2A (0.1 M), H_2PtCl_6 (5 μL, 1 wt.%), H_2O (30 mL), 300 W Xe lamp. Chamber B (hydrogenation reaction): Ethanol (10 mL), alkyne (20 μL), Pd/C (5 mg, 5 wt.%), 80 °C. The conversions were determined by gas chromatography (GC).

The crystalline and chemical structure of COF was retained after the reaction, as confirmed by PXRD, FT-IR and TEM characterizations (Figure S54-57). The AQE for H_2 evolution was calculated as a function of incident light wavelength (Figure 3d). It showed that the maximum AQE of Rubpy-ZnPor COF was 9.68 % at 420 nm, which showed a positive relationship with the UV-vis adsorption spectrum. We then compared the performance with the previously reported COF catalysts used for photocatalytic H_2 evolution, the results showed that the Rubpy-ZnPor COF catalyst is one of the best among the reported COF based photocatalysts to the best of our knowledge (Figure 3e and Table S2).

In view of the high efficiency and sustained high production of H_2 (30338 μmol g^{-1} h^{-1}, 743 mL g^{-1} h^{-1}) for the synthesized Rubpy-ZnPor COF photocatalyst, we believe the further tandem utilized the generated H_2 by converted it into high value added fine organic chemicals will be a meaningful chemical process. Herein, in the following work, we attempted to directly use the photocatalytic generated H_2 for the hydrogenation reaction of unsaturated hydrocarbons (alkyne and alkene). The tandem reactors were homemade by pipeline connecting two glass chambers, thus ensuring the yield H_2 can freely diffuse to the hydrogenation reactor (Figure 4a).

As shown in Figure 4b, the photocatalytic H_2 production in tandem with organic hydrogenation results suggested that the yield H_2 was sufficient to support hydrogenation reactions with >99.9% conversation for phenylacetylene, 4-chlorophenylacetylene, 4-bromophenylacetylene, and 4-methylphenylacetylene hydrogenation. Furthermore, we also evaluated the performance of the olefin's hydrogenation reactions. The conversion efficiency of α-methylstyrene and cyclohexene to corresponding alkanes was achieved at 98.2% and 70.6% when using Rubpy-ZnPor COF photocatalyst to produce H_2 as a reductant source. Overall, this tandem reaction method realized the direct utilization of photocatalytic generated hydrogen to chemical compounds, thus achieving the photocatalytic products upgrade to highly valued organic chemicals.

Based on the precise structure of these COFs, the density functional theory (DFT) calculations based on Rubpy-ZnPor COF as molecular model were conducted to gain insights into the population of excited states and photophysical processes (Figure 5a and S66). We found that, in the excitation process, two major transitions (S0 → S4 and S0 → S6) were located at 2.55 eV and 3.14 eV and the corresponding molecular orbitals were distributed on Rubpy and ZnPor ligands in Rubpy-ZnPor COF. The calculated results reveal that the singlet excited states (SESs) of S4 and S6 were both the charge transfer states as their approximative oscillator strength. The simulated adsorption and emission spectrums are shown in Figure S67. We found the absorption spectrum shows peaks at ~400 and 1000 nm (denoted as S4-6 and S1-S2), which is consistent with the experimental UV-vis spectrum. While for the emission spectrum, those two peaks are broadened, weakened and red shift to 450 nm and 1300 nm and the intensity becomes rather weak. This explains the origin of the one peak in the experimental fluorescence (FL) spectrum. The intersystem crossing (ISC) process has been studied by the triplet calculation and the spin-orbital coupling effect. The SESs of Rubpy-ZnPor COF can efficiently transform into triplet state via an ISC process. The triplet state was localized on the Rubpy unit, which fully agreed with the spin density surfaces (Figure 5b) of Rubpy-ZnPor COF. In addition, T5 and T6 states were populated on both Rubpy and

ZnPor units and then degenerate to T1. It is well known that triplet state will supply longer time for efficient electron transfer between photocatalysts and other components, thus resulting in an efficient process for promoting hydrogen evolution.[8, 10a]

In summary, the photophysical processes of Rubpy-ZnPor COF were rationalized by TD-DFT calculations, confirming the efficient energy excitation and the population of the Rubpy-localized electronic state, which can efficiently trigger the electron transfer to afford further redox reactions. Based on the above experiments and analysis, an intrinsic photocatalytic cycle was proposed to explain the photosensitive process and photocatalytic H_2 evolution mechanism for this COF catalyst (Figure 5c): Under visible light irradiation, both the photosensitive group Rubpy and ZnPor can be excited and subsequently electron transfer proceeded by two different pathways: 1) upon exciting the Rubpy part, the triplet state of Rubpy-ZnPor COF was populated on Rubpy by a photochemical process of [Rubpy]-[ZnPor] → ^{*1}[Rubpy]-[ZnPor] → ^{*3}[Rubpy]-[ZnPor]. 2) upon exciting ZnPor unit, a three-step photophysical process was revealed as follows: [Rubpy]-[ZnPor] → [Rubpy]-[ZnPor]^{*1} →[Rubpy]-[ZnPor]^{*3} →(TTET) ^{*3}[Rubpy]-[ZnPor] (triplet-triplet energy transfer, TTET). After that, Rubpy-localized triplet state of Rubpy-ZnPor COF could accept electron from electron donor to generate the reduced $^{\cdot}$[Rubpy]-[ZnPor], followed by transfer to the active sites (Pt as co-catalyst) for H^+ reduction to H_2. Above all, Rubpy-ZnPor COF with dual-PSs showed binary excitation channels, which can promote light energy conversion and subsequent photocatalytic water splitting.

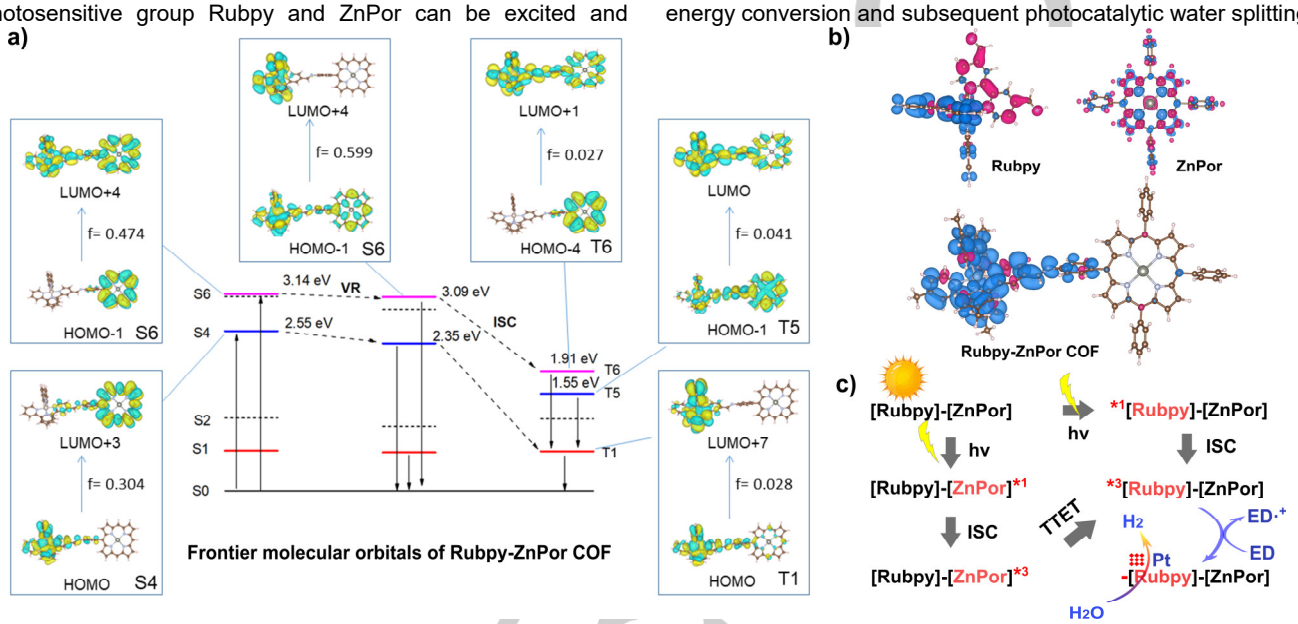

Figure 5. Mechanism and DFT calculations. **a)** Selected frontier molecular orbitals involved in the excitation and singlet excited state/triplet excited state (TES) of Rubpy-ZnPor COF. For clarity, only selected excited states are presented. **b)** Triplet spin density surfaces for Rubpy-ZnPor COF. **c)** Proposed photochemical process for H_2 evolution.

Conclusion

In conclusion, this work innovatively developed a versatile method to couple multiple traditional PSs, mainly $Ru(bpy)_3^{2+}$ and metalloporphyrin by covalent linkage and get a series of dual photosensitive based 3D MCOFs. As expected, these MCOFs combine the properties of strong light-absorbing ability, efficient electron transfer, and suitable band gap for photocatalytic HER. Among them, Rubpy-ZnPor COF achieved the highest H_2 generation rate (30338 μmol g^{-1} h^{-1}) with AQE of 9.68%@420 nm, which showed one of the best performances over reported COF based catalysts. Besides, the in-situ produced H_2 was successfully tandem used for organic hydrogenation reaction due to its sustained high production. Furthermore, the TD-DFT calculation thoroughly demonstrated the photophysical process, where both the Rubpy and ZnPor can be excited and subsequently went through two pathway electron transfer process to get Rubpy-localized electronic state. Thereafter, the dual excitation behaviors promote light-electron conversion and the subsequent highly efficient photocatalytic water splitting to H_2. This work pioneeringly explored the covalently linked of two photosensitizer monomers to construct photoactive COFs, which shows the great potential of using multifold photosensitive heterogeneous materials in the field of photocatalysis, also provides new insight into the design and development of highly efficient photocatalysts.

Acknowledgements

This work was financially supported by NSFC (No. 22225109, 21871141, 22105080, and 22201083) and Project funded by China Postdoctoral Science Foundation (No. 2020M682748 and 2021M701270). China National Postdoctoral Program for Innovative Talents (BX20220115). Guangzhou Basic and Applied Basic Research Fund Project (Grant 202102020209). Research and Cultivation Fund for Young Teachers of South China Normal University (No. 21KJ02).

Keywords: covalent organic framework • dual-photosensitizer • photocatalytic hydrogen evolution • organic hydrogenation

[1] a) T. Banerjee, F. Podjaski, J. Kröger, B. P. Biswal, B. V. Lotsch, *Nat. Rev.Mater.* **2021**, *6*, 168-190; b) I. Sullivan, A. Goryachev, I. A. Digdaya, X. Li, H. A. Atwater, D. A. Vermaas, C. Xiang, *Nature Catalysis* **2021**, *4*, 952-958; c) J. Barber, *Chem. Soc. Rev.* **2009**, *38*, 185-196.

[2] a) Y. Wang, A. Vogel, M. Sachs, R. S. Sprick, L. Wilbraham, S. J. A. Moniz, R. Godin, M. A. Zwijnenburg, J. R. Durrant, A. I. Cooper, J. Tang, *Nature Energy* **2019**, *4*, 746-760; b) L. Marzo, S. K. Pagire, O. Reiser, B. König, *Angew. Chem. Int. Ed.* **2018**, *57*, 10034-10072; c) X. Wang, L. Chen, S. Y. Chong, M. A. Little, Y. Wu, W.-H. Zhu, R. Clowes, Y. Yan,

M. A. Zwijnenburg, R. S. Sprick, A. I. Cooper, *Nat. Chem.* **2018**, *10*, 1180-1189; d) W.-K. Han, Y. Liu, X. Yan, Y. Jiang, J. Zhang, Z.-G. Gu, *Angew. Chem. Int. Ed.* **2022**, e202208791.

[3] a) C. P. Xu, P. R. Anusuyadevi, C. Aymonier, R. Luque, S. Marre, *Chem. Soc. Rev.* **2019**, *48*, 3868-3902; b) Q. Wang, J. Warnan, S. Rodríguez-Jiménez, J. J. Leung, S. Kalathil, V. Andrei, K. Domen, E. Reisner, *Nature Energy* **2020**, *5*, 703-710; c) S. Wang, B. Y. Guan, X. W. D. Lou, *J. Am. Chem. Soc.* **2018**, *140*, 5037-5040.

[4] a) E. Pastor, M. Sachs, S. Selim, J. R. Durrant, A. A. Bakulin, A. Walsh, *Nat. Rev.Mater.* **2022**, *7*, 503-521; b) A. Mehtab, J. Ahmed, S. M. Alshehri, Y. B. Mao, T. Ahmad, *Nanotechnology* **2022**, *33,* 142001; c) J. R. Ran, M. Jaroniec, S. Z. Qiao, *Adv. Mater.* **2018**, *30,* 1704649.

[5] a) H. L. Wang, L. S. Zhang, Z. G. Chen, J. Q. Hu, S. J. Li, Z. H. Wang, J. S. Liu, X. C. Wang, *Chem. Soc. Rev.* **2014**, *43*, 5234-5244; b) Y. X. Fang, Y. D. Hou, X. Z. Fu, X. C. Wang, *Chem. Rev.* **2022**, *122*, 4204-4256.

[6] a) Q. Wang, K. Domen, *Chem. Rev.* **2020**, *120*, 919-985; b) D. F. Swearer, H. Q. Zhao, L. N. Zhou, C. Zhang, H. Robatjazi, J. M. P. Martirez, C. M. Krauter, S. Yazdi, M. J. McClain, E. Ringe, E. A. Carter, P. Nordlander, N. J. Halas, *Proc. Natl. Acad. Sci. U. S. A.* **2016**, *113*, 8916-8920.

[7] a) P. L. Cheung, S. C. Kapper, T. Zeng, M. E. Thompson, C. P. Kubiak, *J. Am. Chem. Soc.* **2019**, *141*, 14961-14965; b) S. Guo, K.-K. Chen, R. Dong, Z.-M. Zhang, J. Zhao, T.-B. Lu, *ACS Catal.* **2018**, *8*, 8659-8670; c) C. V. Krishnan, N. Sutin, *J. Am. Chem. Soc.* **1981**, *103*, 2141-2142; d) A. Jati, K. Dey, M. Nurhuda, M. A. Addicoat, R. Banerjee, B. Maji, *J. Am. Chem. Soc.* **2022**, *144*, 7822-7833; e) T. U. Connell, C. L. Fraser, M. L. Czyz, Z. M. Smith, D. J. Hayne, E. H. Doeven, J. Agugiaro, D. J. D. Wilson, J. L. Adcock, A. D. Scully, D. E. Gómez, N. W. Barnett, A. Polyzos, P. S. Francis, *J. Am. Chem. Soc.* **2019**, *141*, 17646-17658; f) J. Tian, B. Huang, M. H. Nawaz, W. Zhang, *Coord. Chem. Rev.* **2020**, *420*, 213410; g) J. Min Park, J. H. Lee, W.-D. Jang, *Coord. Chem. Rev.* **2020**, *407*, 213157.

[8] a) P. Wang, S. Guo, H.-J. Wang, K.-K. Chen, N. Zhang, Z.-M. Zhang, T.-B. Lu, *Nat. Commun.* **2019**, *10*, 3155; b) J. Zhao, W. Wu, J. Sun, S. Guo, *Chem. Soc. Rev.* **2013**, *42*, 5323-5351.

[9] a) K. K. Chen, S. Guo, H. Y. Liu, X. Y. Li, Z. M. Zhang, T. B. Lu, *Angew. Chem. Int. Ed.* **2020**, *59*, 12951-12957; b) S. Guo, L. Ma, J. Zhao, B. Küçüköz, A. Karatay, M. Hayvali, H. G. Yaglioglu, A. Elmali, *Chem. Sci.* **2014**, *5*, 489-500; c) B. Zheng, R. P. Sabatini, W.-F. Fu, M.-S. Eum, W. W. Brennessel, L. Wang, D. W. McCamant, R. Eisenberg, *P. Natl. Acad. Sci.* **2015**, *112*, E3987-E3996; d) K.-K. Chen, C.-C. Qin, M.-J. Ding, S. Guo, T.-B. Lu, Z.-M. Zhang, *P. Natl. Acad. Sci.* **2022**, *119*, e2213479119.

[10] a) J. Z. Zhao, K. J. Xu, W. B. Yang, Z. J. Wang, F. F. Zhong, *Chem. Soc. Rev.* **2015**, *44*, 8904-8939; b) P. Wang, R. Dong, S. Guo, J. Zhao, Z.-M. Zhang, T.-B. Lu, *National Science Review* **2020**, *7*, 1459-1467.

[11] a) C. T. J. Ferguson, K. A. I. Zhang, *ACS Catal.* **2021**, *11*, 9547-9560; b) Y. Qu, X. Duan, *Chem. Soc. Rev.* **2013**, *42*, 2568-2580; c) H. Chen, H. S. Jena, X. Feng, K. Leus, P. Van Der Voort, *Angew. Chem. Int. Ed.* **2022**, *61*, e202204938; d) G. Zhang, Z.-A. Lan, X. Wang, *Angew. Chem. Int. Ed.* **2016**, *55*, 15712-15727; e) Z. Xie, C. Wang, K. E. deKrafft, W. Lin, *J. Am. Chem. Soc.* **2011**, *133*, 2056-2059.

[12] a) C. X. Zhao, Z. P. Chen, R. Shi, X. F. Yang, T. R. Zhang, *Adv. Mater.* **2020**, *32,* 1907296; b) L. H. Lin, Z. Y. Yu, X. C. Wang, *Angew. Chem. Int. Ed.* **2019**, *58*, 6164-6175.

[13] J. D. Xiao, L. L. Han, J. Luo, S. H. Yu, H. L. Jiang, *Angew. Chem. Int. Ed.* **2018**, *57*, 1103-1107.

[14] a) P. F. Wei, M. Z. Qi, Z. P. Wang, S. Y. Ding, W. Yu, Q. Liu, L. K. Wang, H. Z. Wang, W. K. An, W. Wang, *J. Am. Chem. Soc.* **2018**, *140*, 4623-4631; b) G.-B. Wang, K.-H. Xie, H.-P. Xu, Y.-J. Wang, F. Zhao, Y. Geng, Y.-B. Dong, *Coord. Chem. Rev.* **2022**, *472*, 214774; c) R. Liu, K. T. Tan, Y. Gong, Y. Chen, Z. Li, S. Xie, T. He, Z. Lu, H. Yang, D. Jiang, *Chem. Soc. Rev.* **2021**, *50,* 120-242; d) C. S. Diercks, O. M. Yaghi, *Science* **2017**, *355*, eaal1585; e) M. Lu, M. Zhang, J. Liu, Y. Chen, J.-P. Liao, M.-Y. Yang, Y.-P. Cai, S.-L. Li, Y.-Q. Lan, *Angew. Chem. Int. Ed.* **2022**, *61*, e202200003.

[15] a) M. Lu, J. Liu, Q. Li, M. Zhang, M. Liu, J.-L. Wang, D.-Q. Yuan, Y.-Q. Lan, *Angew. Chem. Int. Ed.* **2019**, *58*, 12392-12397; b) S. Y. Ding, W. Wang, *Chem. Soc. Rev.* **2013**, *42*, 548-568; c) Q. Guan, L.-L. Zhou, Y.-B. Dong, *Chem. Soc. Rev.* **2022**, *51*, 6307-6416; d) J. Dong, X. Han, Y. Liu, H. Li, Y. Cui, *Angew. Chem. Int. Ed.* **2020**, *59*, 13722-13733.

[16] a) O. M. Yaghi, M. O'Keeffe, N. W. Ockwig, H. K. Chae, M. Eddaoudi, J. Kim, *Nature* **2003**, *423*, 705-714; b) H. Jiang, D. Alezi, M. Eddaoudi, *Nat. Rev.Mater.* **2021**, *6*, 466-487; c) N. W. Ockwig, O. Delgado-Friedrichs, M. O'Keeffe, O. M. Yaghi, *Acc. Chem. Res.* **2005**, *38*, 176-182.

[17] a) M. Lu, M. Zhang, J. Liu, T.-Y. Yu, J.-N. Chang, L.-J. Shang, S.-L. Li, Y.-Q. Lan, *J. Am. Chem. Soc.* **2022**, *144*, 1861-1871; b) L. Grill, M. Dyer, L. Lafferentz, M. Persson, M. V. Peters, S. Hecht, *Nat. Nanotechnol.* **2007**, *2*, 687; c) C. Jia, A. Migliore, N. Xin, S. Huang, J. Wang, Q. Yang, S. Wang, H. Chen, D. Wang, B. Feng, Z. Liu, G. Zhang, D.-H. Qu, H. Tian, M. A. Ratner, H. Q. Xu, A. Nitzan, X. Guo, *Science* **2016**, *352*, 1443.

[18] H.-S. Lu, W.-K. Han, X. Yan, C.-J. Chen, T. Niu, Z.-G. Gu, *Angew. Chem. Int. Ed.* **2021**, *60*, 17881-17886.

[19] a) C. Gong, X. Yang, X. Wei, F. Dai, T. Zhang, D. Wang, M. Li, J. Jia, Y. She, G. Xu, Y. Peng, *Materials Chemistry Frontiers* **2023**, *7*, 230-237. b) H. Li, J. Ding, X. Guan, F. Chen, C. Li, L. Zhu, M. Xue, D. Yuan, V. Valtchev, Y. Yan, S. Qiu, Q. Fang, *J. Am. Chem. Soc.* **2020**, *142*, 13334-13338. c) J. Ding, X. Guan, J. Lv, X. Chen, Y. Zhang, H. Li, D. Zhang, S. Qiu, H.-L. Jiang, Q. Fang, *J. Am. Chem. Soc.* **2023**, *145*, 3248-3254.

[20] a) H. M. Rietveld, *J. Appl. Crystallogr.* 1969, 2, 65-71. b) J. Maschita, T. Banerjee, G. Savasci, F. Haase, C. Ochsenfeld, B. V. Lotsch, *Angew. Chem. Int. Ed.* 2020, *59*, 15750-15758. c) L. Grunenberg, G. Savasci, M. W. Terban, V. Duppel, I. Moudrakovski, M. Etter, R. E. Dinnebier, C. Ochsenfeld, B. V. Lotsch, *J. Am. Chem. Soc.* **2021**, *143*, 3430-3438. d) C. Gao, J. Li, S. Yin, J. Sun, C. Wang, *Nat. Commun.* **2020**, *11*, 4919. e) F. Haase, E. Troschke, G. Savasci, T. Banerjee, V. Duppel, S. Dörfler, M. M. J. Grundei, A. M. Burow, C. Ochsenfeld, S. Kaskel, B. V. Lotsch, *Nat. Commun.* **2018**, *9*, 2600.

[21] The cambridge crystallographic cata centre (CCDC) deposition number for Rubpy-2HPor COF and Febpy-2HPor COF are 2266001 and 2252025, respectively. Copies of the data can be obtained free of charge via https://www.ccdc.cam.ac.uk/structures/.

[22] H. L. Nguyen, C. Gropp, Y. Ma, C. Zhu, O. M. Yaghi, *J. Am. Chem. Soc.* **2020**, *142*, 20335-20339.

[23] S. Y. Ding, J. Gao, Q. Wang, Y. Zhang, W. G. Song, C. Y. Su, W. Wang, *J. Am. Chem. Soc.* **2011**, *133*, 19816-19822.

[24] Y. Liu, Y. Ma, J. Yang, C. S. Diercks, N. Tamura, F. Jin, O. M. Yaghi, *J. Am. Chem. Soc.* **2018**, *140*, 16015-16019.

10.1002/anie.202307632

Entry for the Table of Contents

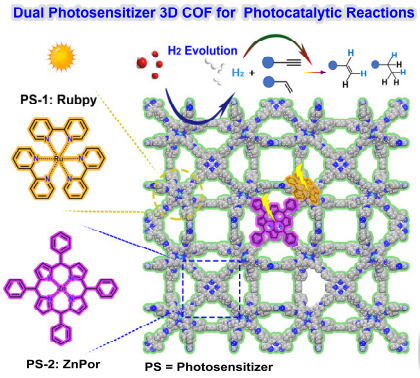

A versatile method allows dual-photosensitizer-based three-dimensional metal-covalent organic framework (3D MCOF) photocatalysts to be built by covalently linking two traditional photosensitizers (pyridine ruthenium and metalloporphyrin complex). These COFs exhibit outstanding activity in photocatalytic hydrogen evolution and the in-situ produced hydrogen can be used in tandem for alkyne hydrogenation.

The following is a personal Twitter handle for social media promotion:

Twitter handle: @langmuir_mi

Twitter name: Meng